Supramolecular Chemistry
Publication details, including instructions for authors and subscription information:
http://www.informaworld.com/smpp/title~content=t713649759

Cholic Acid Inclusion Compounds with Aromatic Ketone Guests: Structure and Reaction Kinetics

Janet L. Scott[a]
[a] Department of Chemistry, University of Cape Town, Rondebosch, South Africa

To cite this Article Scott, Janet L.(1997) 'Cholic Acid Inclusion Compounds with Aromatic Ketone Guests: Structure and Reaction Kinetics', Supramolecular Chemistry, 8: 3, 231 — 239
To link to this Article: DOI: 10.1080/10610279708034940
URL: http://dx.doi.org/10.1080/10610279708034940

SUPRAMOLECULAR CHEMISTRY, 1997, Vol. 8, pp. 231–239
Reprints available directly from the publisher
Photocopying permitted by license only

Cholic Acid Inclusion Compounds with Aromatic Ketone Guests: Structure and Reaction Kinetics

JANET L. SCOTT

Department of Chemistry, University of Cape Town, Rondebosch, 7700, South Africa

(Received 11 December 1996)

The crystal structure of the inclusion compound formed with host cholic acid and guest propiophenone indicates different packing from that seen in other CA-aromatic guest compounds. Space group $P2_1$, a = 16.790(1), b = 7.928(5), c = 12.262(3) Å, β = 114.25(2)°, Z = 2, D_c = 1.211 g.cm^{-3}, R = 0.0515 for 2145 independent reflections. The kinetics of decomposition of the inclusion compounds of the inclusion compounds of CA with acetophenone and propiophenone are presented and mechanism and rate of decomposition compared and contrasted.

The steroidal bile acid (3α, 7α, 12α-trihydroxy-5β-cholan-24-oic acid), commonly known as cholic acid (CA), forms inclusion compounds with a wide range of guest molecules. The crystal structures of the inclusion compounds with water[1,2,3] and alcohol guests[4,5,6] exhibit extensive host-host and host-guest hydrogen bonding. The inclusion compound of CA with acetone and three water molecules is comprised of hydrogen bonded bilayers of host and guest which pack together resulting in a close packed structure[7]. All water molecules and host and guest hydroxyl and carbonyl groups are involved in intermolecular hydrogen bonds of which there are ten per asymmetric unit.

Apart from the above examples and an interesting structure of CA with *m*-fluoro-aniline, which exhibits an unusual 1:2 host:guest ratio and peculiar packing arrangement[8], most CA inclusion compounds form tubulate clathrate type structures. Puckered host steroid bilayers pack together such that channels are formed in which the guest molecules are trapped without benefit of short range host-guest interactions. Bilayers result from the head to tail and α-face to α-face hydrogen bonding of the host while adjacent bilayers are bound by van der Waals forces. Guest molecules included in such fashion encompass lactones,[9,10] benzene[11] and benzene derivatives,[12,13] aliphatic ketones[14] and esters[15].

We have in the past considered the phases occurring during thermal decomposition of various CA inclusion compounds[7] and the different packing modes and subtle guest responsive changes in host conformation and packing occurring[15]. More recently we have undertaken study of the rates and mechanisms of decomposition of CA tubulate clathrates with substituted aromatic guests[16] as well as investigated the solid state reactivity of CA and its O(28) methyl ester, methyl cholate (MC)[17]. We now present the crystal structure of the 1:1 inclusion compound formed by CA with propiophenone (CAPR) and consider the complex thermal decomposition modes of this compound and that formed by CA with acetophenone[13] (CAACET) both with respect to rate and mechanism of reaction. Kinetic parameters are derived and presented for comparison.

EXPERIMENTAL

Single crystals of the inclusion compound were grown by slow cooling of a supersaturated solution of dry CA in propiophenone. The colourless needles obtained were cut to obtain suitable fragments for single crystal diffractometry. Crystals were sealed in Lindemann capillary tubes with mother liquor to prevent desorption of the

guests during data collection. Preliminary cell parameters were obtained photographically and intensity data were collected on an Enraf-Nonius CAD4 diffractometer at 294 K using graphite monochromated Mo-K_α radiation (λ = 0.7107 Å) and the $\omega - 2\theta$ scan mode. Refined unit cell parameters were obtained by least squares analysis of 24 reflections measured on the diffractometer in the range $16 < \theta < 17°$. During data collection three references reflections were monitored periodically to check crystal stability. The data were corrected for Lorentz-polarisation effects. Crystal data and other experimental details are given in Table I.

Structure Solution and Refinement

The crystal structure of the inclusion compound was solved by direct methods using the program SHELX-86[18] and refined by full-matrix, least-squares refinement using the program SHELX-76[19]. The weighting scheme employed was $w = [\sigma^2(F) + 0.0013F_o^2]^{-1}$ chosen to ensure constant distribution of $<w\,(|F_o| - |F_c|)^2>$ with respect to sin θ and $(F_o/F_{max})^{1/2}$ and final R factors were: R = 0.0515 and wR = 0.0575 with S = 1.59 for 2145 independent reflections with $I_{rel} > 2\sigma I_{rel}$ and 338 parameters. After refinement $\Delta\rho_{max}$ = 0.32 eÅ^{-3} and $\Delta\rho_{min}$ = −0.27 eÅ^{-3}. The y coordinate of one non-hydrogen atom of the host was fixed to define the origin in the polar space group $P2_1$. All non-hydrogen atoms of the host were refined anisotropically while those of the guest were refined isotropically. The oxygen atom of the propiophenone guest molecule was modelled as disordered over two sites with the sum of the s.o.f.s constrained to unity. The resultant occupancies were 0.65 for O(1G) and 0.35 for O(1GA). Guest site occupancy factors were restrained to unity (or to sum to unity in the case of disordered groups) as it was deemed unwise to attempt to refine occupancy factors for a guest molecule with high thermal parameters and exhibiting disorder. Hydrogen atoms were placed in geometrically generated positions and refined with positional parameters riding on the host atom with methyl, methylene and methine hydrogen atoms tied to a common temperature fac-

TABLE I Crystal data and experimental parameters for CAPR.

Crystal Data	
Molecular formula	$C_{24}H_{40}O_5 \cdot C_9H_{10}O$
Molecular weight (gmol^{-1})	542.757
Space group	$P2_1$
a(Å)	16.790(1)
b(Å)	7.928(5)
c(Å)	12.262(3)
α(°)	90.0
β(°)	114.25(2)
γ(°)	90.0
V(Å^3)	1488.2(10)
Z	2
D_c(gcm^{-3})	1.211
D_m(gcm^{-3})	1.201(2)
μ(MoKα) (cm^{-1})	0.80
F(000)	592
Data collection	
Crystal dimensions (mm)	0.3 × 0.3 × 0.25
Range, h, k, l	±14, 9, 19
Total exposure time (h)	22.9
Intensity variation(%)	−0.7
No. of reflections collected	2942
No. of reflections $I_{rel} > 2\sigma I_{rel}$	2172

tor for each type and all guest hydrogen atoms tied to a single common temperature factor. Host hydroxyl hydrogen atoms were located in electron density difference maps and refined with simple bond length restraints.

Final fractional atomic coordinates, temperature factors, bond lengths and angles and tables of structure factors have been deposited at the Cambridge Crystallographic Data Centre.

Thermal Analysis

Differential Scanning Calorimetry (DSC) and Thermal Gravimetry (TG) were performed on a Perkin Elmer PC7 system.

Rising temperature thermal analysis: Crystals of the inclusion compounds were removed from mother liquor, blotted dry and lightly crushed before analysis. Sample masses in the range 1–5 mg were analysed in the temperature range 30–230 °C at a heating rate of 20 °C.min^{-1} with dry nitrogen purge gas at a flow rate of 40 cm^3 min^{-1}.

Isothermal thermal analysis: Crystals of the inclusion compounds were grown as for X-ray diffractometry, filtered from the mother liquor, washed with dry diethyl ether to remove any uncomplexed guest, crushed and sieved. The fractions with particle sizes 212–250 μm and 63–125 μm were retained and the powders kept under an atmosphere of the relevant guest to prevent desorption of the guest. The desorption reactions were carried out under isothermal thermogravimetric conditions at temperatures in the ranges indicated in Table II. Resultant weight loss percentage *versus* time curves were converted to extent of reaction (α) *versus* time curves which were fitted to one of the common rate law equations.[20] The best fit was deemed to be that which most nearly approached linearity over the largest α range. Values of the rate constant, *k*, thus obtained were used to produce Arrhenius plots for estimation of the activation energies.

X-ray diffraction: Powder diffraction spectra of the inclusion compounds and of the desolvated material were recorded at 294 K using the continuous scan mode and Cu-K_α radiation. Crystalline samples were crushed and the spectrum recorded over the 2θ range 6–36°. Calculated spectra were produced from crystal structure data using the program LAZYPULVERIX[21] modified to produce gaussian curves instead of lines.

RESULTS

The asymmetric unit consists of one host and guest pair and the conformation of both molecules is indicated in Figure 1. The mode of packing adopted by the CAPR inclusion compound is that of the B-type structures[15] in which the C(19) methyl groups are in close contact about the screw diad at (0, y, 1/2) as is illustrated in the packing diagram, Figure 2. This packing mode is unique amongst structures of the inclusion compounds of CA with aromatic guests and results in a channel with more oval cross sectional shape than the more usual A-type packing which is exhibited in the structure of CA with acetophenone.[13] As in other B-type structures[15] the steroid side chain is in the extended confor-

TABLE II Hydrogen bonding schemes for CAPR

	O●●●O (Å)	O-H (Å)	HO (Å)	O-H●●●O (°)
O(28)●●●O(29)	2.728 (6)	0.97 (6)	1.82 (6)	153.9 (4)
O(29)●●●O(25)	2.683 (8)	0.96 (5)	1.73 (6)	172 (4)
O(25)●●●O(26)	2.882 (6)	0.98 (5)	1.92 (5)	165 (5)
O(26)●●●O(27)	2.812 (8)	0.98 (6)	1.89 (7)	155 (5)

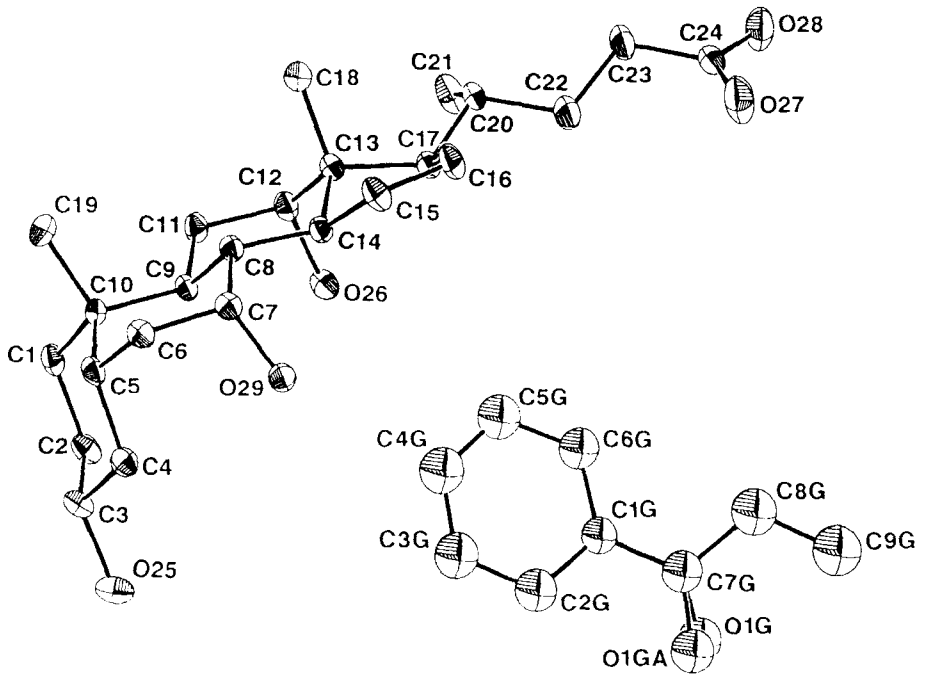

FIGURE 1 Molecular diagram of CAPR showing thermal ellipsoids at 30% probability. Molecular numbering of the host follows conventional steroid numbering.

mation as defined by the torsion angle C(17)-C(20)-C(22)-C(23) = −169.7(5)° (the analogous angle in the A-type structures with puckered side chain conformations is in the range 54–66 °). The familiar puckered steroid bilayers bound together by host-host hydrogen bonding as detailed in Table III are noted and host bond lengths and angles are similar to those found in analogous structures. No short range host-guest interactions occur. It is interesting to note the differences in this structure with propiophenone as guest molecule and that published by Miki *et al* with acetophenone guest.[13] A change in packing mode from A- to B-type structures results although the guest molecules differ by only 1 side chain carbon atom. This change in packing mode, which reflects the change in steroid side-chain configuration, is presumably due to the increased space requirements of the side chain. Attempts to form inclusion compounds with butyrophenone have been unsuccessful and it is possible that this structure represents an approach to the limit of guest size for successful inclusion compound formation without loss of bilayer structure.

The host:guest ratios of both compounds were confirmed by weight loss percent on TG analysis. Measured weight loss % values were very close to those predicted assuming 1: host: guest stoichiometry (CAACET: calc. 22.7%, measured 22.7%; CAPR: calc. 24.7%, measured 24.0%). While rising temperature thermal analysis of these compounds indicates a single guest loss event, rising temperature DSC analysis reveals the occurrence of distinct exotherms directly following the endothermic peak associated with guest loss (Figure 3a and b). In the case of CAPR two endotherms associated with guest loss occur. Microscopic observation of crystals of the compounds under rising temperature and N_2 flow reveal that guest loss is accompanied by partial melting or dissolution of

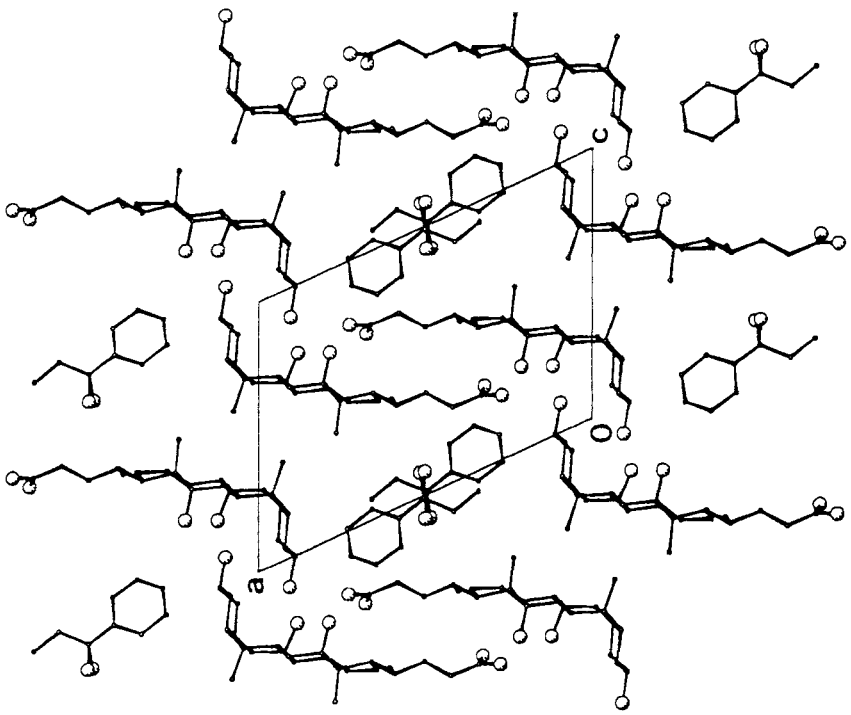

FIGURE 2 Packing diagram of CAPR viewed as a projection down [010]. Oxygen atoms are indicated as larger circles and both positions of O1G are plotted.

the crystals followed by recrystallisation of the CA(α) phase which in turn melts at *ca* 200 °C. The recrystallisation of CA(α) from the melt as the concentration of guest decreases would result in an exothermic thermal event. The double endotherm related to guest loss in the DSC trace of CAPR may be due to a solid phase change similar to that noted in other B-type structures[15]

TABLE III Data for the analysis of decomposition isotherms for CAACET and CAPR.

T(°C)	α-range	k (min^{-1})	r	α-range	k (min^{-1})	r
CAACET						
(linear)				**(B1)**		
80	0.02–0.7	0.0101(2)	0.999			
85	0.005–0.45	0.01753(2)	1.000			
90	0.001–0.36	0.0310(4)	0.999	0.3–0.95	0.2302(6)	0.997
95	0.001–0.2	0.03994(8)	1.000	0.2–0.95	0.4458(9)	0.999
100	0.002–0.20	0.0668(2)	0.999	0.35–0.95	0.0825(2)	0.999
105	0.005–0.18	0.0925(6)	0.998	0.13–0.95	1.114(3)	0.999
110	0.007–0.16	0.118(3)	0.995	0.1–0.95	1.382(6)	0.999
CAPR						
(R3)				**(B1)**		
100	0.05–0.4	0.00750(1)	0.999	0.45–0.95	0.1213(6)	0.995
105	0.05–0.42	0.01195(2)	0.999	0.45–0.95	0.251(1)	0.997
110	0.05–0.4	0.0187(2)	0.994	0.4–0.95	0.477(3)	0.998
115	0.05–0.25	0.0292(1)	0.998	0.3–0.95	0.790(5)	0.994
120	0.05–0.2	0.0413(3)	0.998	0.4–0.95	0.477(3)	0.998

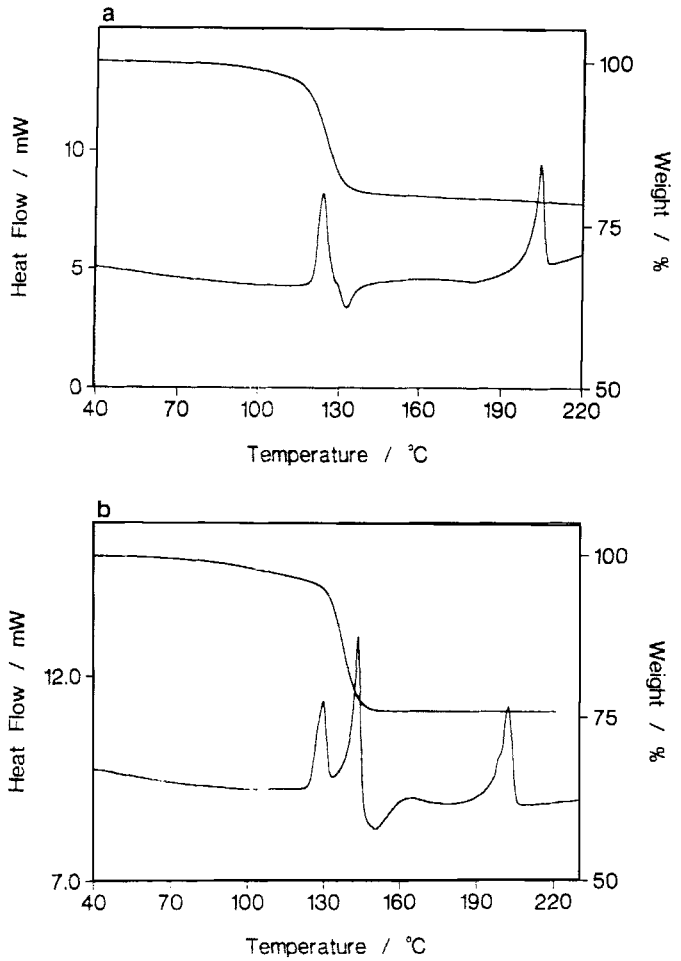

FIGURE 3 TG and DSC traces at heating rates of 20 °Cmin^{-1} for (a) CAACET and (b) CAPR.

but this could not be confirmed as it proved impossible to isolate the phase occurring between this event and the guest loss.

It is important that the measured rates of decomposition under isothermal conditions correspond to the loss of guest from the *solid, crystalline* inclusion compound phase (not from a melt) if any conclusions relating to mechanism are to be drawn. To this end, only decomposition curves obtained at temperatures well below those at which melting became obvious were included in the study. Finely ground samples were examined microscopically at each temperature and no evidence of melting was noted in the ranges used. Powder XRD analysis of the solids remaining after decomposition of the inclusion compound indicates the existence of the CA(α) phase only and no other polymorphs were detected in any of the experiments.

The isothermal decomposition curves of CAPR and CAACET were complex and appear to result from a series of overlapping or succeeding curves due to the predominance of different mechanisms or processes at different stages of the reaction. Careful analysis of the α *versus* time curves for CAACET reveal an initial linear region, which persists to higher α values at lower temperatures, followed by a truncated sigmoidal

curve, the latter indicating overlapping of two separate processes. A number of different possible rate laws were fitted to the second region of the curve after rescaling but regeneration of the α *versus* time curve and comparison of the 1st derivative curves due to the experimental and calculated data indicated that the experimental data are best approximated by a linear region (conforming to a zero order rate law) followed by a region described by a B1 (Prout-Tompkins) rate law. The fit of the calculated and experimental data for decomposition at 85 °C is presented in Figure 4a. Each curve was analysed in this fashion and the rate constants extracted for the first and second processes are presented in Table III.

The isothermal decomposition curves of CAPR are more complex yet, with three distinct regions indicated. The initial region, terminated at low α, appears either linear or deceleratory but was not modelled due to uncertainty in temperature at the beginning of an isothermal TG run. This region is followed by a second, distinctly different, deceleratory region extending

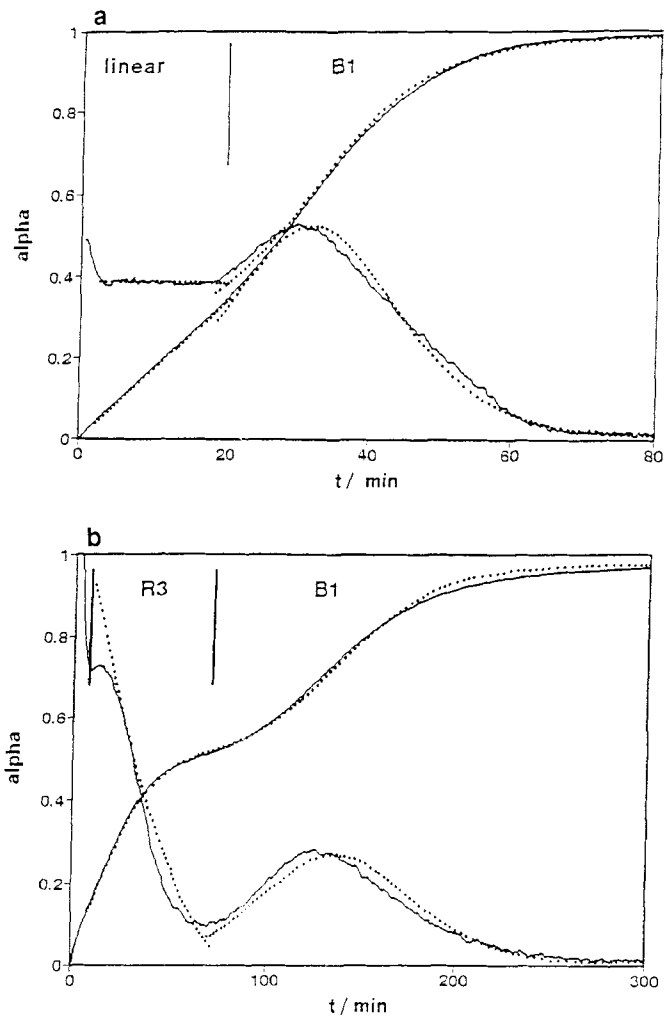

FIGURE 4 Comparison of experimental (solid line) and calculated (dotted line) α vs time and $d\alpha/dt$ curves for (a) CAACET 212–250 μm at 85 °C and (b) CAPR 212–250 μm at 90 °C.

to *ca* $\alpha = 0.4$ which is in turn succeeded by a truncated sigmoidal region as occurs in CAACET. Unlike CAACET the second deceleratory region does not vary in α-range with variations in temperature. The best fit of successive rate laws was achieved by modelling an R3 (contracting volume) mechanism followed by a B1 (Prout-Tompkins) rate law. The fit of calculated and experimental data at 90 °C is illustrated in figure 4b and the rate constants extracted for particular α ranges quoted in Table III.

Arrhenius plots for each discrete part are presented in Figure 5a and b and the kinetic parameters derived therefrom detailed in Table III. It is difficult to validate possible processes which might account for such multi-step behaviour although it is clear that different processes dominate the decomposition of both of these compounds at different stages in the reaction. A plausible mechanism might involve loss of guest from the channels and surfaces as the rate determining step in the initial stages of decomposition and the predominance of the formation and subsequent growth of nuclei of the CA(α) product phase in the latter stages. The values for the activation energies derived for both compounds

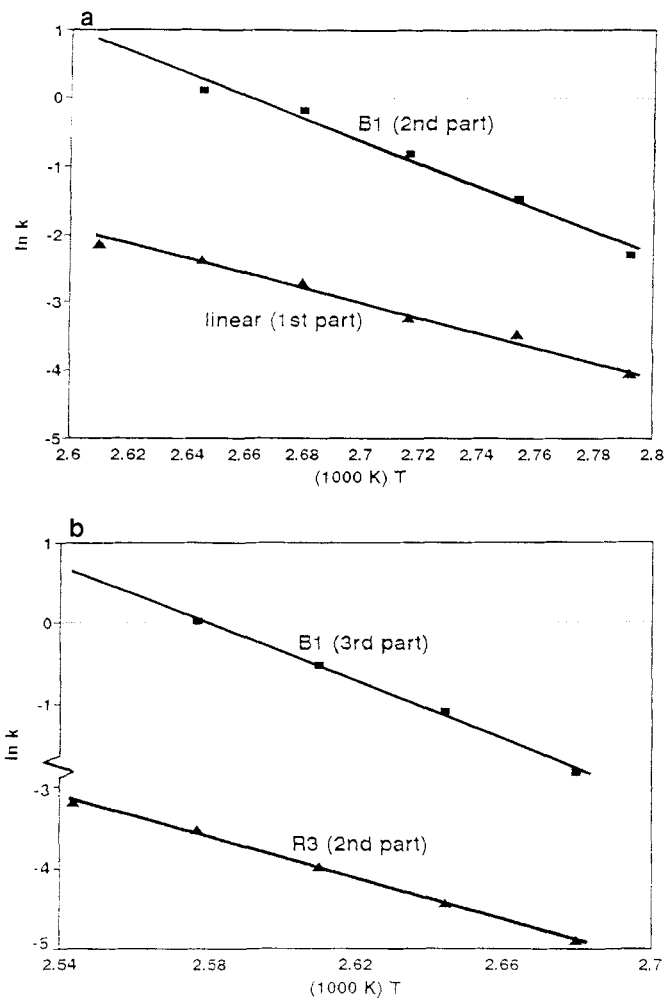

FIGURE 5 Arrhenius plots for CAACET and CAPR over the experimentally determined isokinetic ranges. E_a and ln A values for each distinct process are derived.

TABLE IV Kinetic parameters for CAACET and CAPR.

	E_a (kJmol^{-1})	In A	r
CAACET			
linear region	93(5)	27.01(11)	0.988
Prout-Tompkins (B1)	138(11)	44.15(16)	0.980
CAPR			
Contracting volume (R3)	105(2)	29.02(3)	0.999
Prout-Tompkins (B1)	151(7)	46.60(7)	0.995

are similar for the first and second phases of CAACET and CAPR respectively and are lower than the E_a values derived for the sigmoidal regions of the curves as might be expected if the successive mechanisms postulated above accurately represented the processes occurring.

Interestingly the decomposition behaviour of these inclusion compounds with aromatic ketone guests is markedly different to that noted for CA with nitrobenzene, aniline, *p*-nitro-toluene, *p*-toluidine and benzonitrile guests[16] all of which decay in a single step following a B1 rate law. Thus, in spite of similarities of packing and lack of short range host-guest interactions, different decomposition mechanisms (particularly in the initial stages of reaction) are noted for the compounds containing aromatic ketone guest molecules.

References

[1] Lessinger, L. *Cryst. Struct. Commun.* 1982, **11**, 1787.
[2] Lessinger, L. *Eur. Cryst. Meeting* **1985**, *9*, 417.
[3] Lessinger, L.; Low, B.W. *J. Cryst. Spectrosc. Res.* **1993**, *23*, 85.
[4] Jones, E.L.; Nassimbeni, L.R. *Acta Cryst., B (Str. Sci.)* **1990**, *46*, 399.
[5] Johnson, P.L.; Schaefer, J.P. *Acta Crystallogr., Sect. B* **1972**, *28*, 3083.
[6] Jones, E. L.; Nassimbeni, L. R. *Acta Cryst., B (Str. Sci.)* **1990**, *46*, 399.
[7] Caira, M.R.; Nassimbeni, L.R.; Scott, J.L. *J. Chem. Soc., Perkin Trans. 2* **1994**, 1403.
[8] Shibakami, M. and Sekiya, A. *J. Chem. Soc., Chem. Commun.* **1994**, 429.
[9] Miyata, M.; Shibakami, M. and Takemoto, K. *J. Chem. Soc., Chem. Commun.* **1988**, 655.
[10] Miki, K.; Kasai, N.; Shibakami, M.; Takemoto, K.; Miyata, M. *J. Chem. Soc., Chem. Commun.* **1991**, 1757.
[11] Nakano, K.; Sada, K.; Miyata, M. *Chem. Lett.* **1994**, 137.
[12] Caira, M.R.; Nassimbeni, L.R.; Scott, J.L. *J. Chem. Soc., Chem. Commun.* **1993**, 612.
[13] Miki, K.; Masui, A.; Kasai, N.; Miyata, M.; Shibakami, M.; Takemoto, K. *J. Am. Chem. Soc.* **1988**, *110*, 6594.
[14] Caira, M.R.; Nassimbeni, L.R.; Scott, J.L. *J. Chem. Crystallogr.* **1994**, *24*, 783.
[15] Caira, M.R.; Nassimbeni, L.R.; Scott, J.L. *J. Chem. Soc., Perkin Trans 2* **1993**, 623.
[16] Scott, J.L. *Supramol. Chem.* **1995**, in press.
[17] Scott, J.L. *J. Chem. Soc., Perkin Trans 2.* **1995**, 495.
[18] Sheldrick, G.M., SHELX-86, *Crystallographic Computing* 3, ed. G.M. Sheldrick, C. Kruger and R. Goddard, Oxford University Press, **1985**, p 175.
[19] Sheldrick, G.M., SHELX-76: *A Program for Crystal Structure Determination*, University of Cambridge, Cambridge, UK, **1976**.
[20] Brown, M.E., Introduction to Thermal Analysis, Techniques and Applications. Chapman and Hall, London, **1988**.
[21] Yvon, K.; Jeitschko, W.; Parthé, E. *J. Appl. Cryst.* **1977**, *10*, 73.